# Study of Foveal Avascular Zone Growth in Individuals With Mild Diabetic Retinopathy by Optical Coherence Tomography

Jian Liu,[1,2] Yang He,[1] Linghui Kong,[1] Dongni Yang,[3] Nan Lu,[3] Yao Yu,[1,2] Yuqian Zhao,[1] Yi Wang,[1,2] and Zhenhe Ma[1,2]

[1]School of Control Engineering, Northeastern University at Qinhuangdao, Qinhuangdao City, China
[2]Hebei Key Laboratory of Micro-Nano Precision Optical Sensing and Measurement Technology, Qinhuangdao City, China
[3]Department of Ophthalmology, The First Hospital of Qinhuangdao, Qinhuangdao City, Hebei Province, China

Correspondence: Zhenhe Ma, School of Control Engineering, Northeastern University at Qinhuangdao, No. 143-1, Jianshe Street, Haigang District, Qinhuangdo City, Hebei Province 066004, China; mazhenhe@163.com.

**Received:** April 6, 2023
**Accepted:** August 18, 2023
**Published:** September 12, 2023

Citation: Liu J, He Y, Kong L, et al. Study of foveal avascular zone growth in individuals with mild diabetic retinopathy by optical coherence tomography. *Invest Ophthalmol Vis Sci.* 2023;64(12):21. https://doi.org/10.1167/iovs.64.12.21

**Purpose.** The purpose of this study was to investigate the association between foveal vessels and retinal thickness in individuals with diabetic retinopathy (DR) and control subjects, and to reveal foveal avascular zone (FAZ) growth in early individuals with DR.

**Methods.** The regions with a thickness less than 60 µm were marked from the intima thickness maps and named $FAZ_{Thic}$. The avascular zones extracted from the deep vascular plexus were designated as $FAZ_{Angi}$. The boundary of the two FAZ forms a ring region, which we called $FAZ_{Ring}$. The FAZ growth rate was defined as the ratio of the $FAZ_{Ring}$ area to the $FAZ_{Thic}$ area. Thirty healthy controls and 30 individuals with mild nonproliferative DR were recruited for this study.

**Results.** The $FAZ_{Thic}$ area in individuals with mild DR and control subjects showed similar distribution. The $FAZ_{Angi}$ area in individuals with mild DR are higher than that in control subjects on the whole, but there was no significant difference ($P > 0.05$). The $FAZ_{Ring}$ area in individuals with mild DR was significantly higher than that in control subjects ($P < 0.001$). However, there is still a small amount of overlap data between the two groups. For the FAZ growth rate, the individuals with mild DR were also significantly larger than the control subjects ($P < 0.001$). But there were no overlapping data between the two groups.

**Conclusions.** The growth of FAZ in individuals with mild DR can be inferred by comparing $FAZ_{Angi}$ with $FAZ_{Thic}$. This method minimizes the impact of individual variations and helps researchers to understand the progression mechanism of DR more deeply.

Keywords: foveal avascular zone (FAZ), foveal vessels, retinal thickness, diabetic retinopathy (DR)

Diabetic retinopathy (DR), a common microvascular disease caused by diabetes, is the leading cause of blindness in adults worldwide.[1,2] In its early stages, DR is usually asymptomatic and often goes unnoticed. However, once the disease progresses to an advanced stage, many serious complications can occur, such as diabetic macular edema, vitreous hemorrhage, or retinal detachment.[3] Early diagnosis and timely treatment of DR can help reduce the blindness rate and prevent other retinal complications.[4]

Current diagnostic methods for DR rely primarily on fundus photography (FP) or fluorescent angiography (FA) images.[5–7] Microaneurysms, macular edema, neovascularity, hemorrhage, and exudate are commonly used as biomarkers for the detection and classification of DR.[8] However, FP requires mydriasis and carries a risk of complications, limiting the utility of this technique in elderly individuals.[9] Additionally, the low resolution of capillaries by FP hampers the diagnosis of the disease. FA examination is time-consuming and risky, as some patients injected with contrast agents may experience adverse reactions, such as shock and nausea.[10]

Optical coherence tomography (OCT) is a commonly used diagnostic device in ophthalmology. It has the advantages of high resolution, noninvasive, and fast imaging speed. OCT angiography (OCTA) is a functional imaging technique of OCT that allows for the acquisition of three-dimensional perfusion maps at the capillary level without the requirement of contrast agents.[11] OCT, including OCTA, can serve as a reliable basis for the diagnosis and classification of DR, due to its ability to observe the retinal structure and vascular network in detail, and obtain important information, such as retinal thickness and vascular morphology.[12–14]

The capillary network of the inner retinal layer (IRL) forms a circular area around the fovea with no blood vessels in the center called the fovea avascular zone (FAZ). The FAZ is a natural feature of retinal development and can be observed in individuals without retinal pathology.[15] However, in the case of DR, FAZ undergoes changes over time or with disease progression. The enlargement of the FAZ is positively correlated with the severity of DR.[16] Studies

have shown that individuals with mild to moderate nonproliferative DR have a smaller FAZ growth rate, whereas individuals with proliferative DR have a larger FAZ growth rate.[17,18] Thus, the FAZ growth rate might be a hallmark feature of DR occurrence and progression.

However, several studies by entopic perception,[19,20] OCT,[21,22] and adaptive optics ophthalmoscopy[23–25] have shown considerable interindividual variation (0.02 $mm^2$ to 0.63 $mm^2$) in FAZ size and shape in control subjects. The substantial interindividual variations in the FAZ impose limitations on numerous scientific investigations.[26,27] Moreover, these differences significantly impact the accuracy of disease diagnosis. Although the FAZ area in subjects with DR is significantly larger compared to control subjects at a group level, there is a possibility of misdiagnosis when relying solely on the FAZ area due to individual variations. Therefore, mitigating the influence of individual variations is a prerequisite for studying the FAZ growth in subjects with DR.

The structure of the IRL in the macular central region exhibits a pit shape, which is an important natural feature, formed during retinal development. Springer et al. demonstrated, through the establishment of a retinal model, that the fovea pit is formed due to the absence of a vascular syste.[28–30] The absence of blood vessels renders the tissue more elastic, making it more prone to deformation. During the development of the retina, the tissue within FAZ undergoes thinning due to the combined effects of intraocular pressure (IOP) and stretching, resulting in the formation of a pit. The density and distribution of blood vessels also influence the arrangement and differentiation of cells in the retina.[31] During development, neural cells migrate from the central foveal region toward the periphery, forming the fovea pit, and the extent of this migration is matched with the metabolic support provided by the capillaries.[32,33] On the other hand, retinal capillaries provide nutrients and oxygen to the IRLs, maintaining their normal functions and metabolism.[34] It is not possible to have a thick retina without sufficient vascular support.[35]

A study by Chui et al.,[35] demonstrated that the critical diffusion distance of capillaries is approximately 30 µm. Therefore, in healthy eyes, regions with an IRL thickness greater than 60 µm are expected to have capillary oxygen supply. The thickness of the IRL at the edge of the FAZ remained constant at 60 µm regardless of the size of the FAZ area. Thus, alterations in FAZ due to disease can be assessed by comparing the position of the FAZ boundary with the location of the 60 µm thickness.[35]

The consistency between IRL thickness and the boundaries of the FAZ has been widely recognized; however, the presence of the Henle fiber layer (HFL) beneath the outer plexiform layer (OPL), which is highly influenced by the incident light position and angle, can lead to the blurring of the OPL layer boundaries.[36–38] Wang et al. used ganglion cell complex (GCC) thickness as a surrogate for IRL thickness to determine the theoretical baseline edge of the FAZ.[39,40] In this paper, we utilized an improved deep learning algorithm based on Unet++ to improve the segmentation accuracy of the IRL layer. Additionally, we investigated the correlation between macular vessel and IRL thickness in individuals with DR and control subjects. First, a modified U-Nent ++ network was used to extract the IRL and generate an intima thickness map. Areas with thickness less than 60 µm were marked from the intima thickness map and named $FAZ_{Thic}$. Then, the avascular zone was extracted from the deep capillary plexus image obtained by OCTA and named $FAZ_{Angi}$. The boundary of the two FAZ forms a ring region, which we called $FAZ_{Ring}$. The FAZ growth rate was defined as the ratio of the $FAZ_{Ring}$ area to the $FAZ_{Thic}$ area. The FAZ growth rate is minimally influenced by individual variations, making it a reliable indicator to infer the expansion of the FAZ in individuals with mild DR.

## Methods

### Subjects and Data Acquisition

In this study, 30 healthy controls and 30 individuals with mild nonproliferative DR (NPDR) were recruited. Mild NPDR was defined following the second stage of the International Clinical Diabetic Retinopathy Disease Severity Scale.[41] All subjects were recruited from the First Hospital of Qinhuangdao. The study was conducted in accordance with the principles of the Declaration of Helsinki and received approval from the Institutional Review Board of The First Hospital of Qinhuangdao and the Ethics Committee of Northeastern University Bio and Medical (NEU-EC-2023B008S). Informed consent was obtained from all participants. The inclusion criteria were as follows: (1) participants should have a best-corrected visual acuity (BCVA) of 20/20 or better, be over 18 years old, be healthy or with type 2 diabetes mellitus confirmed by a diabetologist; (2) individuals with DR should not exhibit more than mild NPDR; (3) no history of other ocular diseases or significant media opacity, no previous intraocular treatment (laser, intravitreal injections, cataract surgery, and vitreoretinal surgery), refractive error less than 4 diopters; and (4) no ischemic heart disease, hypertension, or neurodegenerative disease.

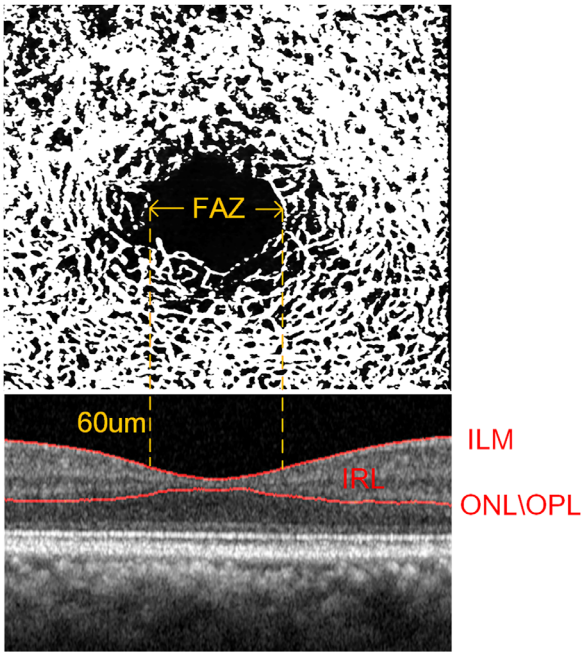


**Figure 1.** Schematic diagram of the foveal avascular zone (FAZ) and IRL thickness. In healthy eyes, the thickness of the IRL at the edge of the FAZ remained constant at 60 µm. ILM, internal limiting membrane; IRL, inner retinal layer; ONL, outer nuclear layer; OPL, outer plexiform layer. The tissue between the two *red lines* is the IRL.

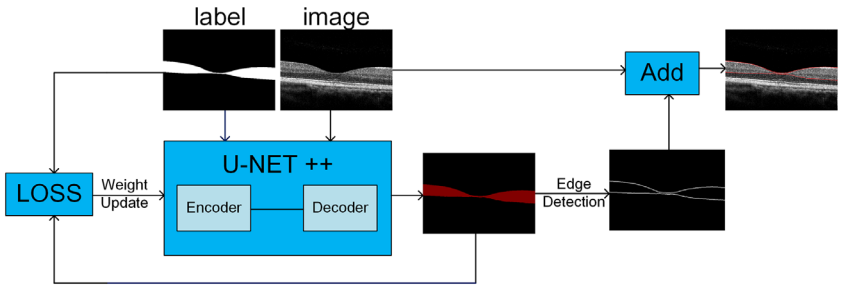


**Figure 2.** Segmentation algorithm of IRL based on deep learning. The label and image were input into the U-net++ network for training. The labels were obtained through manual segmentation. The U-net++ adopts the "Encoder-Decoder" structure. After segmentation, boundary detection was performed on the resulting IRL region, and then overlaid on the original image.

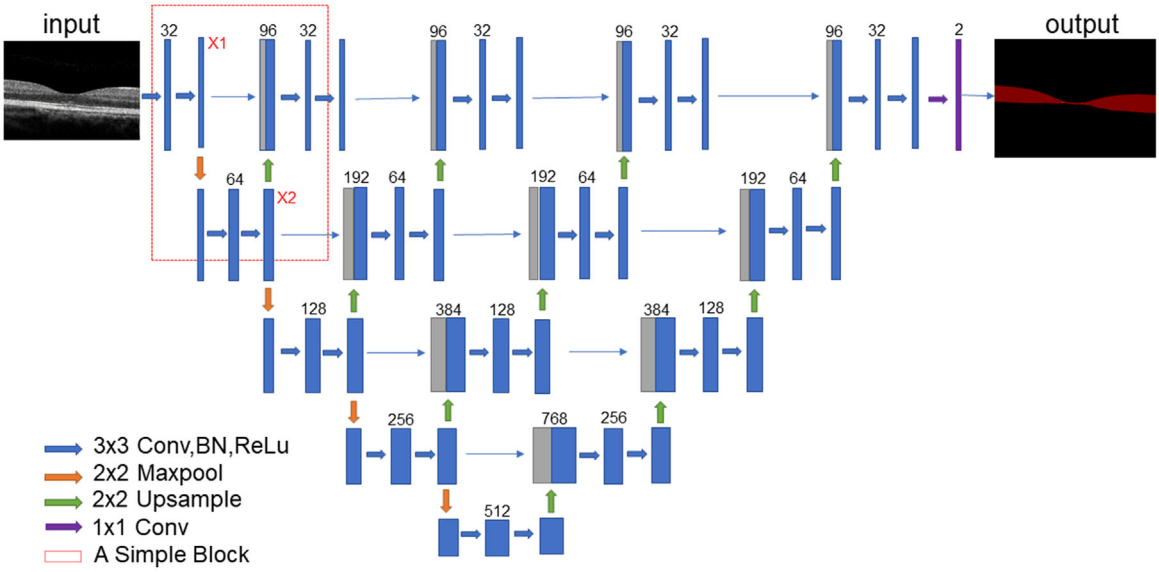


**Figure 3.** U-Net++ network model. The *blue arrow* represents the 3 × 3 convolution operation, the *orange arrows* represent maximum pooling, and the *purple arrow* represents the 1 × 1 convolution operation. The *red dashed box* in Figure 3 shows a basic "Encoder-Decoder" structure unit.

The retinal OCT images used in this study were obtained from a commercial Spectralis OCT system (Heidelberg, Germany). This device operates at an 85 kHz A-scan rate, with a central wavelength of 870 nm and a bandwidth of 50 nm, providing a 3.9-$\mu$m axial and 6-$\mu$m lateral resolution. The ocular light power exposure was within the American National Standards Institute safety limit.[42] OCTA images were obtained by repeating four B-scans on one position and performing decorrelation operations on these B-scans. A complete volume scan consists of 512 B-scan positions. The OCTA volume data were automatically segmented into superficial vascular plexus (SVP) and deep vascular plexus (DVP).

Studies have shown a negative correlation between the area of OCT fundus images and the axial length of the eye.[43] Therefore, it is necessary to correct the size of the fundus images before analyzing their area. We used Bennett's formula[44] to determine the scaling factor (SF): SF = 3.382 × 0.013062 × (AL-1.82). Where AL represents the axial length of the subjects, measured using the Lenstar LS 900. The actual area of the OCT and OCTA images were obtained by multiplying their measured area by the scaling factor. Figure 1 illustrates a schematic diagram of the FAZ and IRL thickness.

## Segmentation Algorithm of IRL Based on Deep Learning

Figure 2 shows the segmentation algorithm of IRL based on deep learning. The 3000 OCT B-scan images (352 × 480) were manually segmented by professional doctors as labels, and randomly divided into the training set and verification set according to a ratio of 7:3.

We chose to segment the region of the IRL rather than its boundaries because doing so helps reduce the disparity in the number of target pixels and background pixels, effectively avoiding the issue of the model being biased toward classifying more pixels as background (i.e. class imbalance). After segmentation, boundary detection was performed on the resulting IRL region, and the distance between the

**Table.** Performance of Different Loss Functions

| Loss Function | IoU Background | IoU Target | IoU Mean | DSC |
|---|---|---|---|---|
| $Loss_{Dice}$ | 0.982 | 0.888 | 0.935 | 0.939 |
| $Loss_{Dice}$+$Loss_{ce}$ | 0.987 | 0.921 | 0.954 | 0.960 |
| $Loss_{Dice}$+$Loss_{ce\_side}$ | **0.988** | **0.930** | **0.959** | **0.964** |

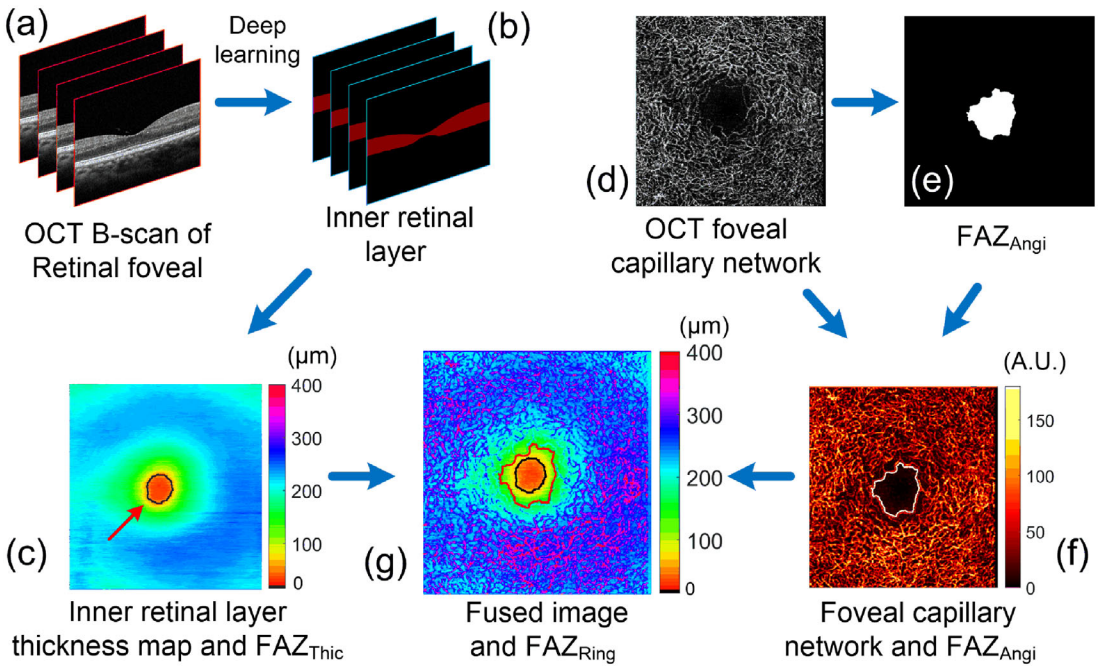


**Figure 4.** Calculation method of FAZ growth. (**a**) OCT B-scan images of retina macular region. (**b**) The segmented IRL. (**c**) The intima thickness map and the location of $FAZ_{Thic}$. (**d**) OCT angiogram. (**e**) $FAZ_{Angi}$ extracted from **d**. (**f**) OCT angiogram and the boundary of $FAZ_{Angi}$. (**g**) The fused image of **c** and **f**.

boundaries was calculated to generate an intima thickness map.

The U-Net++ network structure and specific details are shown in Figure 3. The blue arrow represents the convolution operation, where the convolution kernel size is 3 × 3, the step length is 1, and the image size remains unchanged before and after convolution. The network adopts the "Encoder-Decoder" structure. The red dashed box in Figure 3 shows a basic "Encoder-Decoder" structure unit. Two convolution operations were performed on the input image to obtain X1. The X2 was obtained by performing the down-sampling operation on X1. Then, X1 and X2 were fused. The X2 needed to be up-sampled before fusion. Similar operations were used for other feature fusions in the network.

The traditional U-Net++ network usually uses the Dice Loss function for the semantic segmentation of medical images.[45] The Dice Loss function is shown in Equation 1.

$$Loss_{Dice} = 1 - \frac{2\sum_{i=1}^{c} g_i y_i + \epsilon}{\sum_{i=1}^{c} g_i^2 + \sum_{i=1}^{c} y_i^2 + \epsilon} \tag{1}$$

where C is the batch size, $p_i$ and $g_i$ represent the output image and the label image, respectively, and $\varepsilon = 0.0001$ is a smoothing factor to prevent the divisor from being zero. However, when using the Dice Loss function to update the network weights, the target region will be more protected, whereas the background part may be ignored. Due to the blurred borders on the left and right sides of the OCT retinal image, the network optimized with Dice Loss tends to mistake the background region for the target region, resulting in over-segmentation errors on both sides of the image.

Cross Entropy (CE) is another Loss function commonly used in classification problems, as shown in Equation 2. Its shortcoming is poor predictive performance in the case of class imbalance. Classes with fewer pixels are more likely to be overlooked. On the problem of retinal inner layer segmentation, CE Loss tends to make the inner layer thickness thinner.

$$Loss_{ce} = -\frac{1}{C}\frac{1}{M}\frac{1}{N}\sum_{i=1}^{C}\sum_{j=1}^{M}\sum_{k=1}^{N}[g_{jk} log y_{jk} + (1 - g_{jk}) \log (1 - y_{jk})] \tag{2}$$

where C is the batch size, $M$ and $N$ represent rows and columns of image, respectively, and $y_{jk}$ and $g_{jk}$ represent the pixel in row $j$ and column $k$ of the output image and label image, respectively. The combination of these two Loss functions (Dice and CE) can achieve complementary advantages. To enhance the segmentation accuracy on both sides of the image, we introduced an improved CE Loss function $Loss_{ce\_side}$. This function imposes an over-segmentation penalty on pixels on both sides of the image in a pixel-by-pixel manner, as shown in Equation 3.

$$Loss_{ce\_side} = -\frac{1}{C}\frac{1}{M}\frac{1}{N}\sum_{i=1}^{C}\left[w_1\sum_{j=1}^{M}\sum_{k=1}^{L} f(g_{jk}, y_{jk}) + w_2\sum_{j=1}^{M}\sum_{k=L+1}^{N-L} f(g_{jk}, y_{jk}) + w_3\sum_{j=1}^{M}\sum_{k=N-L+1}^{N} f(g_{jk}, y_{jk})\right] \tag{3}$$

where $f(g_{jk}, y_{jk}) = g_{jk} log y_{jk} + (1 - g_{jk}) \log(1 - y_{jk})$. $L$ is the length over which the over segmentation penalty is aggravated on both sides. In this paper, $L$ was set to a quarter of the number of image columns. The final network Loss function used in this paper is $Loss = Loss_{Dice} + Loss_{ce\_side}$. The weighting parameters w1, w2, and w3 were set to 1.2, 0.8,

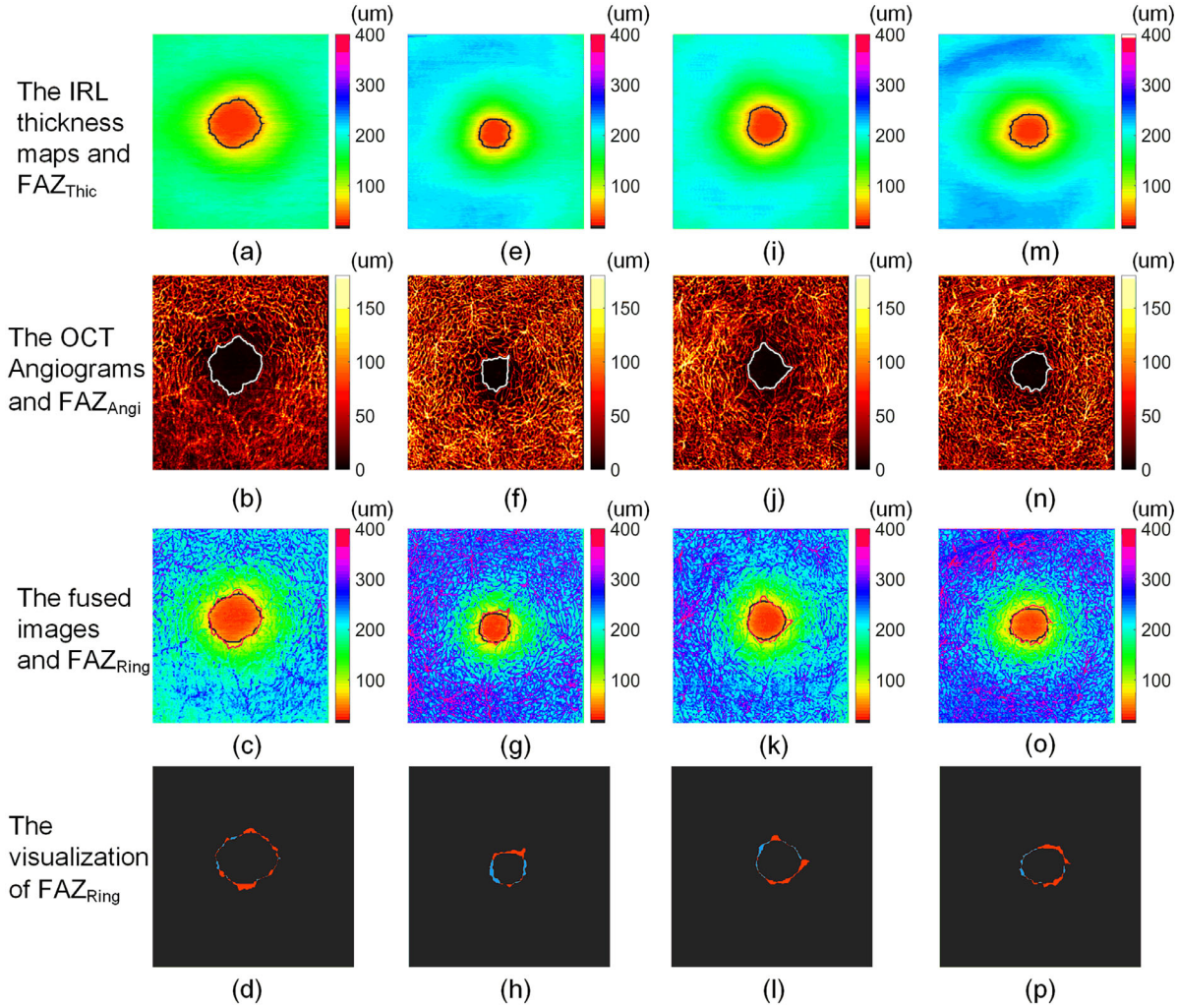


**Figure 5.** The FAZ$_{Thic}$, FAZ$_{Angi}$, and FAZ$_{Ring}$ in control subjects. Each column of images represents an independent subject. The first row shows the intima thickness maps and the FAZ$_{Thic}$, the second row shows the OCT angiograms and the FAZ$_{Angi}$, and the third row shows the fused images and the FAZ$_{Ring}$. The fourth row represents the differences between the FAZ$_{Thic}$ and FAZ$_{Angi}$. The regions where the FAZ$_{Thic}$ exceeds FAZ$_{Angi}$ are displayed in *blue*, whereas the regions where the FAZ$_{Angi}$ exceeds FAZ$_{Thic}$ are displayed in *red*.

and 1.2, respectively. These optimal weighting coefficients were determined through multiple tests.

Two criteria, Intersection over Union (IoU) and Dice Similarity Coefficient (DSC), were used to evaluate the segmentation accuracy of the IRL. IoU is a method to calculate the proportion of different images overlapping each other, as shown in Equation 4. DSC is a method to measure the similarity of two samples, as shown in Equation 5.

$$\mathrm{IoU} = \frac{|\mathrm{A} \cap \mathrm{B}|}{|\mathrm{A} \cup \mathrm{B}|} \tag{4}$$

$$\mathrm{DSC} = \frac{2\,|A \cap B|}{|A| + |B|} \tag{5}$$

where A represents the label image and B represents the network output image.

It can be seen from the Table, that when using the boundary optimization joint loss function $Loss_{Dice}$+$Loss_{ce\_side}$, the segmentation effect reaches the best state.

## Segmentation of FAZ$_{Angi}$ From OCT Angiogram

The second step is to extract the avascular zone from the OCT angiogram using adaptive watershed algorithm[46] combined with an active contour algorithm. Briefly, the original image was first processed with denoising techniques, including Median filtering and Gaussian filtering with 3 × 3 template sizes, and then a region growing algorithm was used to extract the initial FAZ$_{Angi}$ from the denoised image. This initial area is usually much larger than the actual FAZ$_{Angi}$ size. Next, the initial region underwent a distance transformation operation, and then it was inverted, resulting in a topographic map; the watershed algorithm was used to divide the topographic map into several regions. In general, the FAZ is delineated as a contiguous region. However, if the FAZ is divided into multiple subregions, a long boundary line will exist between these regions. To address this, we used a method that detects the length of the boundary line to determine whether these regions are part of the FAZ. If the length of the boundary exceeds a certain threshold, the regions on both sides of the boundary are merged. The

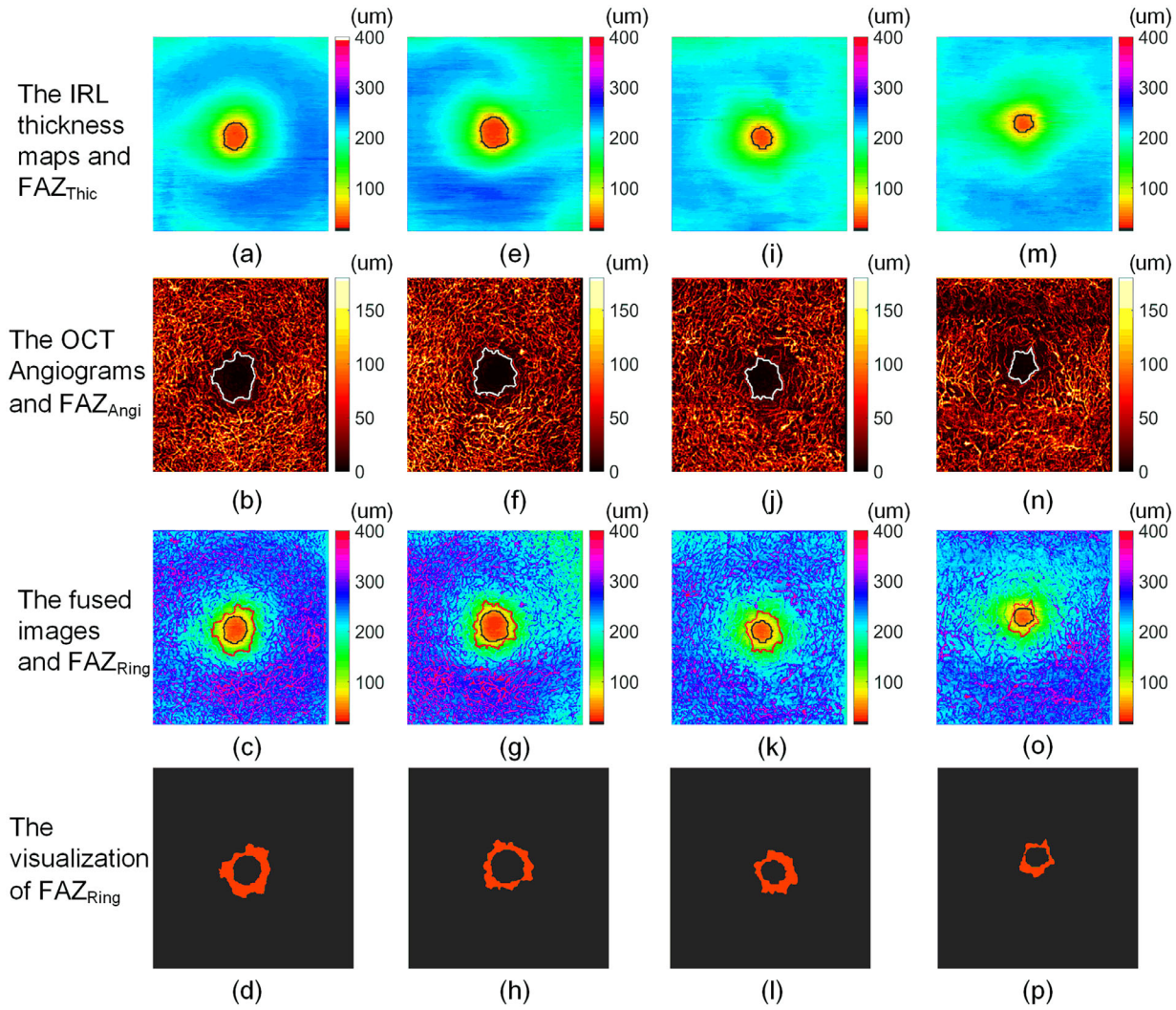


**Figure 6.** The $FAZ_{Thic}$, $FAZ_{Angi}$, and $FAZ_{Ring}$ in individuals with mild DR. Each column of images represents an independent subject. The first row shows the intima thickness maps and the $FAZ_{Thic}$, the second row shows the OCT angiograms and the $FAZ_{Angi}$, and the third row shows the fused images and the $FAZ_{Ring}$. The fourth row represents the difference between the $FAZ_{Thic}$ and $FAZ_{Angi}$, which is referred to as the $FAZ_{Ring}$.

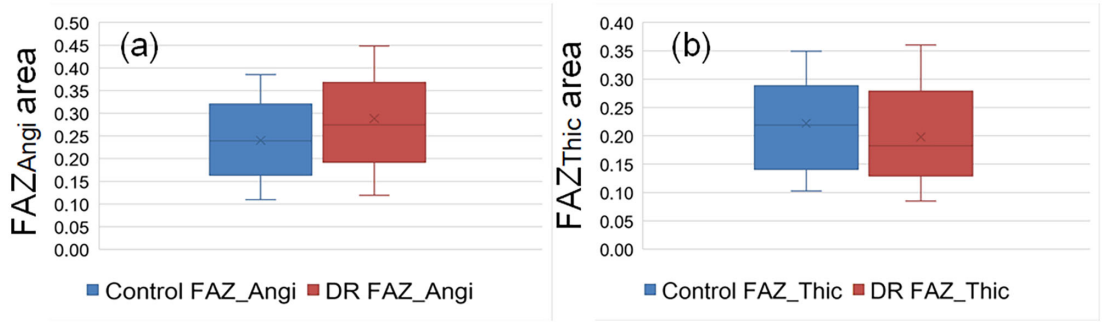


**Figure 7.** Statistical analysis of the $FAZ_{Angi}$ area (**a**) and the $FAZ_{Thic}$ area (**b**) in control subjects and individuals with DR.

threshold is defined as the radius of the largest inscribed circle within the $FAZ_{Angi}$, which represents the maximum value obtained through distance transformation within the FAZ. Although the region obtained by the adaptive watershed algorithm is very close to the real result, the boundary of the region is not smooth enough.[47] The active contour algorithm is very suitable for fine adjustment of the local boundary,[48] especially when the initial boundary is close to

Investigative Ophthalmology & Visual Science

the real result. Therefore, the active contour algorithm was used to further optimize the boundary of the region in this paper.

### Calculation Method of FAZ Growth

The whole process of FAZ growth calculation is shown in Figure 4. The OCT data were obtained from a representative individual with DR.

Figure 4a is OCT B-scan images of the retina macular region, and Figure 4b is the segmented IRL. Figure 4c shows the intima thickness map of the IRL. The blue circle indicated by the red arrow is the position where the thickness is 60 µm. The area enclosed by the circle was named $FAZ_{Thic}$. Figure 4d shows an OCT angiogram of DVP in the retina macular region. The avascular zone is shown in Figure 4e. This region was named $FAZ_{Angi}$ due to its extraction from the OCT angiogram. The edge of the $FAZ_{Angi}$ was extracted and superimposed on the OCT angiogram to obtain Figure 4f. Finally, the Figures 2c and 2f was overlaid on one image. The $FAZ_{Thic}$ represents the theoretical area of the subjects without disease, whereas $FAZ_{Angi}$ represents the actual area of the subjects after disease. These two regions form an annular region which is called the $FAZ_{Ring}$ ($FAZ_{Ring} = FAZ_{Angi} - FAZ_{Thic}$). The $FAZ_{Ring}$ can be regarded as the capillaries change of the subject due to DR. The ratio of the $FAZ_{Ring}$ area to the $FAZ_{Thic}$ area was named FAZ growth rate (FAZ growth = $FAZ_{Ring}$ / $FAZ_{Thic}$).

## Results

Figure 5 shows the results for control subjects and Figure 6 for individuals with mild DR. Each column of images represents an independent subject.

The first row shows the intima thickness map and the position of 60 µm thickness, termed $FAZ_{Thic}$. The second row represents images of DVP in the macular region of the retina and the corresponding $FAZ_{Angi}$. The third row represents the fused images of them both. The fourth row represents the differences between the $FAZ_{Thic}$ and $FAZ_{Angi}$. The regions where the $FAZ_{Thic}$ exceeds the $FAZ_{Angi}$ are displayed in blue, whereas the regions where the $FAZ_{Angi}$ exceeds the $FAZ_{Thic}$ are displayed in red. It can be seen that the $FAZ_{Thic}$ and the $FAZ_{Angi}$ almost coincide in the control subjects in Figure 5. However, in Figure 6, the $FAZ_{Angi}$ has a certain degree of expansion relative to the $FAZ_{Thic}$ in individuals with mild DR. A ring-shaped area is formed between the two, which is the $FAZ_{Ring}$. From the fourth row in Figure 6, it can be observed that due to the $FAZ_{Thic}$ being completely contained within the $FAZ_{Angi}$, there are only red regions in the image. The area of this region corresponds to the area of the $FAZ_{Ring}$.

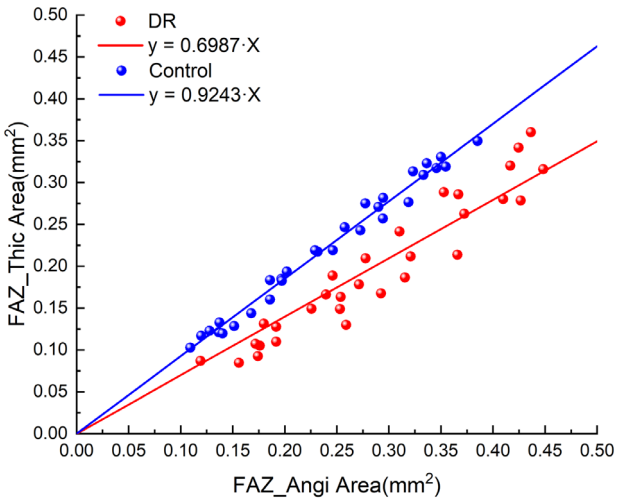


**Figure 8.** The relationship between the $FAZ_{Thic}$ and $FAZ_{Angi}$ for each individual. Each *dot* in Figure 8 represents a subject. *Blue* are the control subjects and *red* are the individuals with DR. The abscissa is the $FAZ_{Angi}$, and the ordinate is the $FAZ_{Thic}$. Each of the two sets of scatter points is fitted to a straight line through the origin.

To better understand the difference between the $FAZ_{Thic}$ and the $FAZ_{Angi}$ in control subjects and individuals with DR, we performed statistical analysis of the data using boxplots. First, we presented the statistical results using the $FAZ_{Angi}$ alone. As described earlier, the mean $FAZ_{Angi}$ of individuals with DR is greater than that of control subjects in a large sample.[49] The results of this paper also support this conclusion, as shown in Figure 7a. Red boxes indicate statistics of the $FAZ_{Angi}$ area in individuals with DR and blue boxes indicate those in control subjects. The red box is slightly higher than the blue box. Due to individual differences, the upper and lower limits of the red and blue boxes fluctuated greatly, and the healthy and diseased boxes overlap in a large area. The *t*-test results show no significant difference in the $FAZ_{Angi}$ between control subjects and individuals with mild DR ($P > 0.05$).

Based on Figure 6, we have known that there are differences between the $FAZ_{Thic}$ and $FAZ_{Angi}$ in individuals with mild DR. However, is this difference due to the $FAZ_{Angi}$ expansion or the $FAZ_{Thic}$ reduction? To answer this question, we also counted the distribution of the $FAZ_{Thic}$ area in control subjects and individuals with DR, as shown in Figure 7b. The results showed that there was no significant difference between them. This indicates that the retinal structure of individuals with early DR does not change significantly, and the location of 60 µm is not significantly different from that of control subjects. This suggests that the large difference between the $FAZ_{Thic}$ and the $FAZ_{Angi}$ in individuals with DR is mainly derived from the enlargement of the $FAZ_{Angi}$, that is, the damage of macular blood vessels.

We used a scatter plot to illustrate the relationship between the $FAZ_{Thic}$ and the $FAZ_{Angi}$ for each individual, as shown in Figure 8. Each dot in Figure 8 represents a subject. Blue are the control subjects and red are the individuals with DR. The abscissa is the $FAZ_{Angi}$, and the ordinate is the $FAZ_{Thic}$. Each of the two sets of scatter points is fitted to a straight line through the origin. The areas of the $FAZ_{Thic}$ and the $FAZ_{Angi}$ in control subjects are very close, so the angle is close to 45 degrees (the slope is close to 1). However, in individuals with DR, the $FAZ_{Thic}$ was significantly smaller than the $FAZ_{Angi}$; therefore, the angle of the line is reduced (the slope is less than 1).

By subtracting the $FAZ_{Thic}$ from the $FAZ_{Angi}$ to obtain the area of the $FAZ_{Ring}$, we counted the difference in the $FAZ_{Ring}$ area between control subjects and individuals with DR, and the results are shown in Figure 9a. It can be seen that the area of the $FAZ_{Ring}$ in individuals with DR is significantly larger than that in control subjects ($P < 0.001$). The FAZ growth rate is defined as the ratio of the $FAZ_{Ring}$ to the $FAZ_{Thic}$. Figure 9b shows the difference in FAZ growth rate between control subjects and individuals with DR. The FAZ growth rate of control subjects are distributed between 0 and 20%, whereas the FAZ growth rate of individuals with

Investigative Ophthalmology & Visual Science

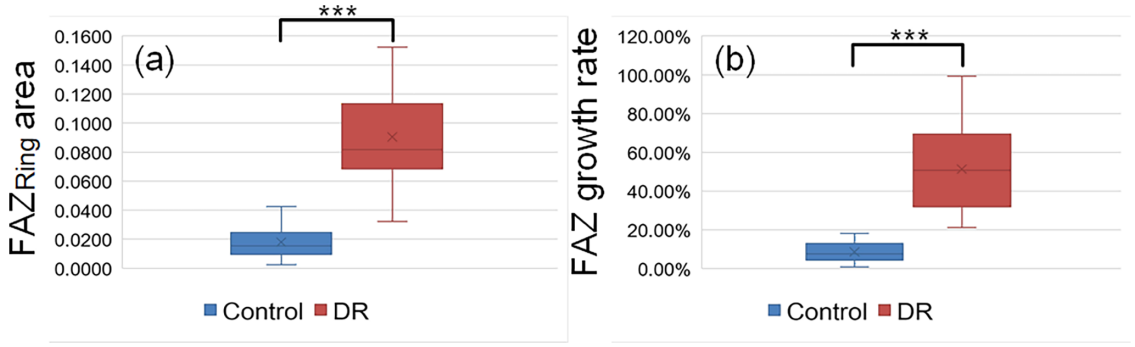


**Figure 9.** The $FAZ_{Ring}$ area (**a**) and the FAZ growth rate (**b**) in control subjects and individuals with DR. ***Represent $P < 0.001$.

mild DR is distributed between 20 and 100%. There is also a significant difference between control subjects and individuals with DR ($P < 0.001$). It is important to note that the FAZ growth rates of control subjects and individuals with DR did not overlap.

## Discussion

Clinical manifestations of DR typically appear 10 to 20 years after the diagnosis of type 2 diabetes or 5 to 10 years after the diagnosis of type 1 diabetes.[50] However, many studies have shown that pathological changes in the retina occur many years before the onset of clinical symptoms.[51,52] Therefore, to protect vision from damage, it is important to diagnose DR early, before clinical manifestations appear.

At present, several methods have been used for the early diagnosis of DR. For example, various molecular content abnormalities caused by DR can be used as the basis for the diagnosis of early DR.[53–56] Among medical imaging methods, FP, FA, and OCT are commonly used to observe DR markers near the macular area of the retina.[57] Vessel density is also used as an early marker of DR.[58] Although the above indicators are helpful for the early detection of DR, capillary occlusion is considered to be a highly valuable early symptom of DR.[59]

The key step in determining the theoretical baseline boundary of the FAZ using the information of IRL thickness is the precise segmentation of the IRL. In this study, we developed an improved Unet++ deep learning algorithm that effectively addresses this problem. We invited expert physicians to manually segment the IRL as training labels. After training on a large dataset, the network achieved an IoU of 0.954 and a DSC of 0.960. When applying the network to clinical data segmentation, we had physicians inspect each segmented result. The proportion of accurately segmented IRL reached 98.3%. We selected images with significant segmentation errors for necessary manual corrections. Once segmentation was completed for all B-scans, we combined the thickness data at all locations to generate a two-dimensional thickness map. On the thickness map, residual errors were mitigated through techniques such as median filtering and mean filtering.

Next, we compared the differences in four parameters ($FAZ_{Angi}$ area, $FAZ_{Thic}$ area, $FAZ_{Ring}$ area, and FAZ growth rate) between two groups of subjects (control subjects and individuals with DR). We obtained the following results: (1) there was no significant difference between the $FAZ_{Angi}$ area and the $FAZ_{Thic}$ area in individuals with mild DR. This suggests that, due to individual differences, the $FAZ_{Angi}$ area alone cannot be used for early detection of DR. (2) There was no significant difference in the $FAZ_{Thic}$ area between individuals with mild DR and control subjects (see Fig. 7b). This indicates no significant changes in retinal structure in individuals with mild DR. (3) The $FAZ_{Ring}$ areas were significantly higher in individuals with mild DR than in control subjects in general (see Fig. 9a). Because there was no significant change in the $FAZ_{Thic}$ area, the increase in the $FAZ_{Ring}$ area was mainly due to the increase in the $FAZ_{Angi}$ area. However, we found that there were still individual data points overlapping in Figure 9a. Therefore, we proposed the concept of the FAZ growth rate. (4) The FAZ growth rate of individuals with mild DR was significantly greater than that of control subjects, its significance was greater than that of the $FAZ_{Ring}$ area, and there was no overlapping data between the two groups (Fig. 9b). This indicates that the FAZ growth rate can provide sufficient sensitivity to help researchers study the DR progression in an individual patient.

Our study also has limitations. The proposed method is more suitable for the diagnosis of early DR, because there are no obvious changes in retinal structure, no macular edema, and other complications in this stage of DR. This ensures that the structure of the IRL is highly identifiable and does not vary significantly in thickness.

### *Acknowledgments*

Supported in part by National Natural Science Foundation of China (61901100 and 62075037), Hebei Provincial Natural Science Foundation of China (E2020501029 and F2020501040).

It was a concerted effort by ophthalmologists and visual science experts to make the work run smoothly.

Disclosure: **J. Liu**, None; **Y. He**, None; **L. Kong**, None; **D. Yang**, None; **N. Lu**, None; **Y. Yu**, None; **Y. Zhao**, None; **Y. Wang**, None; **Z. Ma**, None

### *References*

1. Yamada M, Hiratsuka Y, Roberts CB, et al. Prevalence of visual impairment in the adult Japanese population by cause and severity and future projections. *Ophthalmic Epidemiol*. 2010;17:50–57.
2. Yau JW, Rogers SL, Kawasaki R, et al. Global prevalence and major risk factors of diabetic retinopathy. *Diabetes Care*. 2012;35:556–564.
3. Cheung N, Wong TY. Diabetic retinopathy and systemic vascular complications. *Prog Retin Eye Res*. 2008;27:161–176.

4. Liu L, Chen L. Awareness of diabetic retinopathy is the key step for early prevention, diagnosis and treatment of this disease in China. *Patient Educ Couns*. 2014;94:284–285.
5. Dong B, Wang X, Qiang X, et al. A multi-branch convolutional neural network for screening and staging of diabetic retinopathy based on wide-field optical coherence tomography angiography. *Irbm*. 2022;43:614–620.
6. Li X, Jiang Y, Zhang J, Li M, Luo H, Yin S. Lesion-attention pyramid network for diabetic retinopathy grading. *Artif Intell Med*. 2022;126:102259.
7. Wu Z, Shi G, Chen Y, et al. Coarse-to-fine classification for diabetic retinopathy grading using convolutional neural network. *Artif Intell Med*. 2020;108:101936.
8. Tsiknakis N, Theodoropoulos D, Manikis G, et al. Deep learning for diabetic retinopathy detection and classification based on fundus images: a review. *Comput Biol Med*. 2021;135:104599.
9. Bartlett H, Eperjesi F. Use of fundus imaging in quantification of age-related macular change. *Surv Ophthalmol*. 2007;52:655–671.
10. Kornblau IS, El-Annan JF. Adverse reactions to fluorescein angiography: a comprehensive review of the literature. *Surv Ophthalmol*. 2019;64:679–693.
11. Baran U, Wang RK. Review of optical coherence tomography based angiography in neuroscience. *Neurophotonics*. 2016;3:010902.
12. Liu G, Xu D, Wang F. New insights into diabetic retinopathy by OCT angiography. *Diabetes Res Clin Pract*. 2018;142:243–253.
13. Mahjoub A, Cherni I, Khayrallah O, et al. Contribution of optical coherence tomography angiography OCT-A in diabetic maculopathy. *Ann Med Surg (Lond)*. 2021;70:102904.
14. Yasin Alibhai A, Moult EM, Shahzad R, et al. Quantifying microvascular changes using OCT angiography in diabetic eyes without clinical evidence of retinopathy. *Ophthalmol Retina*. 2018;2:418–427.
15. Balaratnasingam C, Inoue M, Ahn S, et al. Visual acuity is correlated with the area of the foveal avascular zone in diabetic retinopathy and retinal vein occlusion. *Ophthalmology*. 2016;123:2352–2367.
16. Niestrata-Ortiz M, Fichna P, Stankiewicz W, Stopa M. Enlargement of the foveal avascular zone detected by optical coherence tomography angiography in diabetic children without diabetic retinopathy. *Graefes Arch Clin Exp Ophthalmol*. 2019;257:689–697.
17. Kim IG, Lee JE. Optical coherence tomography-angiography: comparison of the foveal avascular zone between diabetic retinopathy and normal subjects. *J Korean Ophthalmol Soc*. 2017;58:952–959.
18. Lynch G, Romo JSA, Linderman R, et al. Within-subject assessment of foveal avascular zone enlargement in different stages of diabetic retinopathy using en face OCT reflectance and OCT angiography. *Biomed Opt Express*. 2018;9:5982–5996.
19. Bradley A, Applegate RA, Zeffren BS, van Heuven WA. Psychophysical measurement of the size and shape of the human foveal avascular zone. *Ophthalmic Physiol Opt*. 1992;12:18–23.
20. Yap M, Gilchrist J, Weatherill J. Psychophysical measurement of the foveal avascular zone. *Ophthalmic Physiol Opt*. 1987;7:405–410.
21. Kurokawa K, Sasaki K, Makita S, Yamanari M, Cense B, Yasuno Y. Simultaneous high-resolution retinal imaging and high-penetration choroidal imaging by one-micrometer adaptive optics optical coherence tomography. *Opt Express*. 2010;18:8515–8527.
22. Wang Q, Kocaoglu OP, Cense B, et al. Imaging retinal capillaries using ultrahigh-resolution optical coherence tomography and adaptive optics. *Invest Ophthalmol Vis Sci*. 2011;52:6292–6299.
23. Chui TY, Zhong Z, Song H, Burns SA. Foveal avascular zone and its relationship to foveal pit shape. *Optom Vis Sci*. 2012;89:602.
24. Dubis AM, Hansen BR, Cooper RF, Beringer J, Dubra A, Carroll J. Relationship between the foveal avascular zone and foveal pit morphology. *Invest Ophthalmol Vis Sci*. 2012;53:1628–1636.
25. Tam J, Martin JA, Roorda A. Noninvasive visualization and analysis of parafoveal capillaries in humans. *Invest Ophthalmol Vis Sci*. 2010;51:1691–1698.
26. Krawitz BD, Mo S, Geyman LS, et al. Acircularity index and axis ratio of the foveal avascular zone in diabetic eyes and healthy controls measured by optical coherence tomography angiography. *Vis Res*. 2017;139:177–186.
27. Ramkumar S, Sasi G. Detection of diabetic retinopathy using OCT image. *Mater Today Proc*. 2021;47:185–190.
28. Springer AD, Hendrickson AE. Development of the primate area of high acuity. 1: use of finite element analysis models to identify mechanical variables affecting pit formation. *Vis Neurosci*. 2004;21:53–62.
29. Springer AD, Hendrickson AE. Development of the primate area of high acuity. 2: quantitative morphological changes associated with retinal and pars plana growth. *Vis Neurosci*. 2004;21:775–790.
30. Springer AD, Hendrickson AE. Development of the primate area of high acuity, 3: temporal relationships between pit formation, retinal elongation and cone packing. *Vis Neurosci*. 2005;22:171–185.
31. Provis JM, Sandercoe T, Hendrickson AE. Astrocytes and blood vessels define the foveal rim during primate retinal development. *Invest Ophthalmol Vis Sci*. 2000;41:2827–2836.
32. Pakzad-Vaezi K, Keane PA, Cardoso JN, Egan C, Tufail A. Optical coherence tomography angiography of foveal hypoplasia. *Br J Ophthalmol*. 2017;101:985–988.
33. Tick S, Rossant F, Ghorbel I, et al. Foveal shape and structure in a normal population. *Invest Ophthalmol Vis Sci*. 2011;52:5105–5110.
34. Lutty GA, McLeod DS. Development of the hyaloid, choroidal and retinal vasculatures in the fetal human eye. *Prog Retin Eye Res*. 2018;62:58–76.
35. Chui TYP, VanNasdale DA, Elsner AE, Burns SA. The association between the foveal avascular zone and retinal thickness. *Invest Ophthalmol Vis Sci*. 2014;55:6870–6877.
36. Lujan BJ, Roorda A, Knighton RW, Carroll J. Revealing Henle's fiber layer using spectral domain optical coherence tomography. *Invest Ophthalmol Vis Sci*. 2011;52:1486–1492.
37. Cense B, Wang Q, Lee S, et al. Henle fiber layer phase retardation measured with polarization-sensitive optical coherence tomography. *Biomed Opt Express*. 2013;4:2296–2306.
38. Otani T, Yamaguchi Y, Kishi S. Improved visualization of Henle fiber layer by changing the measurement beam angle on optical coherence tomography. *Retina*. 2011;31:497–501.
39. Wang BJ, Camino A, Pi SH, et al. Three-dimensional structural and angiographic evaluation of foveal ischemia in diabetic retinopathy: method and validation. *Biomed Opt Express*. 2019;10:3522–3532.
40. Wartak A, Augustin M, Haindl R, et al. Multi-directional optical coherence tomography for retinal imaging. *Biomed Opt Express*. 2017;8:5560–5578.
41. Wilkinson CP, Ferris FL, Klein RE, et al. Proposed international clinical diabetic retinopathy and diabetic macular edema disease severity scales. *Ophthalmology*. 2003;110:1677–1682.
42. Z136 Committee. Laser Institute of America. *American National Standards Institute for Safe Use of Lasers*. New York, NY: American National Standards Institute; 1993.


Investigative Ophthalmology & Visual Science

43. Llanas S, Linderman RE, Chen FK, Carroll J. Assessing the use of incorrectly scaled optical coherence tomography angiography images in peer-reviewed studies a systematic review. *JAMA Ophthalmol*. 2020;138:86–94.
44. Li M, Yang Y, Jiang H, et al. Retinal microvascular network and microcirculation assessments in high myopia. *Am J Ophthalmol*. 2017;174:56–67.
45. Milletari F, Navab N, Ahmadi S-A. V-net: fully convolutional neural networks for volumetric medical image segmentation. *2016 Fourth International Conference on 3D Vision (3DV)*: IEEE; 2016:565–571.
46. Liu J, Yan S, Lu N, et al. Automatic segmentation of foveal avascular zone based on adaptive watershed algorithm in retinal optical coherence tomography angiography images. *J Innov Opt Health Sci*. 2021;15:2242001.
47. Silva AG, Fouto MS, da Silva AT, et al. Segmentation of foveal avascular zone of the retina based on morphological alternating sequential filtering. *2015 IEEE 28th International Symposium on Computer-Based Medical Systems (CBMS)*; 2015:38–43.
48. Diaz M, Novo J, Cutrin P, Gomez-Ulla F, Penedo MG, Ortega M. Automatic segmentation of the foveal avascular zone in ophthalmological OCT-A images. *PLoS One*. 2019;14:e0212364.
49. Al-Sheikh M, Akil H, Pfau M, Sadda SR. Swept-source OCT angiography imaging of the foveal avascular zone and macular capillary network density in diabetic retinopathy. *Invest Ophthalmol Vis Sci*.2016;57:3907–3913.
50. Cho NH. Q&A: five questions on the 2015 IDF Diabetes Atlas. *Diabetes Res Clin Pract*. 2016;115:157–159.
51. Roy S, Kern TS, Song B, Stuebe C. Mechanistic insights into pathological changes in the diabetic retina: implications for targeting diabetic retinopathy. *Am J Pathol*. 2017;187:9–19.
52. Kobrin Klein BE. Overview of epidemiologic studies of diabetic retinopathy. *Ophthalmic Epidemiol*. 2007;14:179–183.
53. Elbana KA, Salem HM, Fattah NRA, Etman E. Serum pentraxin 3 level as a recent biomarker of diabetic retinopathy in Egyptian patients with diabetes. *Diabetes Metab Syndr*. 2019;13:2361–2364.
54. Helal HG, Rashed MH, Abdullah OA, Salem TI, Daifalla A. MicroRNAs (– 146a,– 21 and– 34a) are diagnostic and prognostic biomarkers for diabetic retinopathy. *Biomed J*. 2020;44:S242–S251.
55. Wang X, Zhang M, Li T, Lou Q, Chen X. Effect of urinary albumin creatinine ratio on type 2 diabetic retinopathy and is cut-off value for early diabetic retinopathy diagnosis. *Prim Care Diabetes*. 2022;16:698–702.
56. Chen M, Curtis T, Stitt A. Advanced glycation end products and diabetic retinopathy. *Curr Med Chem*. 2013;20:3234–3240.
57. Kollias AN, Ulbig MW. Diabetic retinopathy: early diagnosis and effective treatment. *Dtsch Arztebl Int*. 2010;107:75–83; quiz 84.
58. Nesper PL, Roberts PK, Onishi AC, et al. Quantifying microvascular abnormalities with increasing severity of diabetic retinopathy using optical coherence tomography angiography. *Invest Ophthalmol Vis Sci*. 2017;58:307–315.
59. Safi H, Safi S, Hafezi-Moghadam A, Ahmadieh H. Early detection of diabetic retinopathy. *Surv Ophthalmol*. 2018;63:601–608.


Investigative Ophthalmology & Visual Science